J. Differential Equations 250 (2011) 2601–2623

Contents lists available at ScienceDirect

Journal of Differential Equations

www.elsevier.com/locate/jde

A geometric mechanism of diffusion: Rigorous verification in a priori unstable Hamiltonian systems ☆

Amadeu Delshams [a,*], Gemma Huguet [b,c]

[a] Dep. de Matemàtica Aplicada I, Universitat Politècnica de Catalunya, Av. Diagonal 647, 08028 Barcelona, Spain
[b] Centre de Recerca Matemàtica, Campus de Bellaterra, Edifici C, 08193 Bellaterra (Barcelona), Spain
[c] Center for Neural Science, New York University, 4 Washington Place, New York, NY 10003, United States

ARTICLE INFO

Article history:
Received 15 July 2010
Revised 29 December 2010
Available online 7 January 2011

ABSTRACT

In this paper we consider a representative a priori unstable Hamiltonian system with $2 + 1/2$ degrees of freedom and we apply the geometric mechanism for diffusion introduced in [A. Delshams, R. de la Llave, T.M. Seara, A geometric mechanism for diffusion in Hamiltonian systems overcoming the large gap problem: heuristics and rigorous verification on a model, Mem. Amer. Math. Soc. 179 (844) (2006), viii + 141 pp.], and generalized in [A. Delshams, G. Huguet, Geography of resonances and Arnold diffusion in a priori unstable Hamiltonian systems, Nonlinearity 22 (8) (2009) 1997–2077]. We provide explicit, concrete and easily verifiable conditions for the existence of diffusing orbits.

The simplification of the hypotheses allows us to perform the straightforward computations along the proof and present the geometric mechanism of diffusion in an easily understandable way. In particular, we fully describe the construction of the scattering map and the combination of two types of dynamics on a normally hyperbolic invariant manifold.

1. Introduction

The goal of this paper is to apply the geometric mechanism for diffusion introduced in [14] and generalized in [12], to a representative a priori unstable Hamiltonian system with $2 + 1/2$ degrees of freedom, establishing explicit conditions for diffusion.

☆ Supported in part by MICINN-FEDER MTM2009-06973 and CUR-DIUE 2009SGR859 grants.
* Corresponding author.
E-mail addresses: Amadeu.Delshams@upc.edu (A. Delshams), gh707@nyu.edu (G. Huguet).

0022-0396/$ – see front matter
doi:10.1016/j.jde.2010.12.023

The phenomenon of global instability in nearly integrable Hamiltonian systems, called commonly *Arnold diffusion*, deals with the changes in the dynamics that take place when an autonomous integrable mechanical system is subject to a small periodic perturbation. More precisely, whether the small periodic perturbations accumulate over time leading to a large term effect or whether they average out.

For an integrable Hamiltonian system written in action-angle variables, all the trajectories lie on invariant tori, with associated dynamics consisting of a rigid rotation with constant frequency. For a general perturbation of size ε of a non-degenerate integrable Hamiltonian, the KAM theorem (see [23] for a survey) ensures stability for most of the trajectories of the system. More precisely, those invariant tori in the unperturbed system $\varepsilon = 0$ having *Diophantine frequencies* are preserved (they are tori with *non-resonant* frequencies), giving rise to a Cantorian foliation of invariant tori for the perturbed system $\varepsilon > 0$. Thus, the set of surviving tori has a large measure but also many gaps among them, which turn out to be of size up to order $\sqrt{\varepsilon}$. However, nothing is said by the KAM theorem about the stability of the trajectories that do not lie on the *non-resonant invariant tori*. Besides, for systems with more than two degrees of freedom the invariant tori are not anymore an obstruction for the existence of trajectories that may possibly drift arbitrarily far, called *diffusing orbits*.

The first description of this instability phenomenon was given by Arnold in [1] for a particular example. Since then, it has been widely studied using a wide range of techniques: geometric, variational and topological (see [11] for a long list of references).

In [1], Arnold considered a particular Hamiltonian consisting of an integrable part with a hyperbolic component (a rotor and a pendulum uncoupled) and a periodic in time perturbation. The perturbation was chosen to preserve the complete foliation of whiskered tori existing in the unperturbed system. Using this foliation, he was able to construct a *transition chain*. A transition chain is a finite sequence of transition tori, that is, *whiskered tori* (invariant tori with associated whiskers: a stable and an unstable manifold) having *non-resonant frequencies* and transverse heteroclinic trajectories between them, that is, the unstable manifold of each transition torus intersects transversally the stable manifold of the next one. Using a topological argument, he proved that diffusing orbits exist in a neighborhood of the tori in a transition chain.

Nevertheless, a generic perturbation creates gaps of size $\sqrt{\varepsilon}$ in the foliation of *primary KAM tori* (whiskered tori which are just a continuation of the whiskered tori that existed in the unperturbed case). These gaps are bigger than the size ε of the heteroclinic intersection between their whiskers predicted by first order perturbation theory. Therefore, one cannot construct straightforwardly a transition chain using only primary KAM tori. This is known in the literature as the *large gap problem* and has been solved very recently by different methods [13,14,12,8,9,26,24,20,19].

In this paper we focus on the *geometric mechanism for diffusion* [14,12]. The strategy in [14,12] to overcome the *large gap problem* was to incorporate in the *transition chain* other invariant objects which are not present in the unperturbed system. They are created in the resonances, filling the gaps between two primary KAM tori. Among these new invariant objects there are the so-called *secondary KAM tori*, which are whiskered tori topologically different from the primary ones. The *scattering map* [15] is the essential tool to study the heteroclinic connections between invariant objects like primary or secondary KAM tori.

In [14] it was proved the existence of Arnold diffusion in *a priori unstable Hamiltonian systems* of $2 + 1/2$ degrees of freedom, under concrete geometric hypotheses. However, one of the hypotheses was the assumption of a non-generic condition, namely, that the Hamiltonian was a trigonometric polynomial in the angular variables. This latter assumption was removed in [12] and the conditions required for the geometric mechanism of diffusion were proven to be $\mathcal{C}^2$-generic for $\mathcal{C}^r$ perturbations of a priori unstable Hamiltonians systems with $2 + 1/2$ degrees of freedom, provided that r is large enough. Moreover, the removal of the trigonometric polynomial hypothesis allowed us to present the conditions for diffusion explicitly in terms of the original perturbation.

The geometric mechanism of diffusion relies on the existence of a *normally hyperbolic invariant manifold* (NHIM), which is an invariant object that organizes the dynamics. This NHIM has associated stable and unstable invariant manifolds that, generically, intersect transversally. Therefore, we can associate to this object two types of dynamics: the *inner* and the *outer* one. The outer dynamics takes into account the asymptotic motions to the NHIM and is described by the *scattering map*. The inner

dynamics is the one restricted to the NHIM and contains Cantor families of primary and secondary KAM tori. The inner and the outer dynamics are combined to construct a transition chain.

A strong feature of the geometric mechanism of diffusion, in contrast to other existing ones, is that the conditions for diffusion are computable and therefore verifiable in specific examples. Moreover, the mechanism provides an explicit description of the diffusing orbits, making it suitable for applications (see [16]).

Although the conditions are explicit, the computations to check them can be harsh in some cases. They may involve, among others, the application of several steps of the averaging method, the expansion in ε of an NHIM, and the verification of the existence of non-degenerate critical points of the Melnikov potential along some straight lines. For clarity of exposition, we have reduced the technical computations to those who were strictly necessary for the comprehension of the mechanism. Thus, we have chosen for this paper a representative class of a priori unstable Hamiltonian systems usually found with several variations in the literature (see Section 2 for references and a discussion of the simplification). This particular choice has two main advantages: (i) the hypotheses provided in [14,12] to apply the geometric method are trivially fulfilled; and (ii) the existence of non-degenerate homoclinic orbits to the NHIM and the inner and outer dynamics to the NHIM can be fully described.

More precisely, we would like to highlight the following accomplishments:

1. The general condition provided by Proposition 3.1 for the existence of transversal intersections among stable and unstable manifolds of the NHIM is geometrically described in Proposition 3.3 and an extremely simple sufficient condition is provided in (11).
2. There exist several transversal intersections leading to different *homoclinic manifolds* of the NHIM. Two of them are *primary* and they can be easily identified. See Remark 3.4.
3. We can identify a maximal domain H in the NHIM for a primary homoclinic manifold. See Eqs. (34) and (35).
4. We provide an explicit expression (41) for the scattering map. It is given by the $-\varepsilon$ time of the flow of a Hamiltonian $\mathcal{L}^*$, called the *reduced Poincaré function*, which is autonomous in the same variables in which the Hamiltonian defining the inner dynamics is readily expressed.

The main result of this paper is Theorem 2.1, which states the existence of Arnold diffusion for a representative type of a priori unstable Hamiltonian system with $2 + 1/2$ degrees of freedom, under concise and easily verifiable hypotheses.

Although this paper strongly relies on the results obtained in the previous papers [14,12], we have made an effort to make it self-contained for the reader just interested in a heuristic description of the mechanism and how it can be applied to concrete examples. We accompany the exposition with precise references to the results in [14,12] for the reader concerned about the rigorous proofs for more general systems.

In particular, we do not need to quote the hypotheses **H1–H3** stated in Theorem 2.1 of [12] (or alternatively, the hypotheses **H1–H5** in [14]). However, for the readers of [14,12] let us mention that hypothesis **H1** is trivially fulfilled by the choice of the potential (3), which is the potential of a classical pendulum.

Hypothesis **H2′** is satisfied with a domain H defined in (34) and guarantees the existence of a homoclinic manifold given in (35). Hypothesis **H2″** is a direct consequence of Proposition 3.9, which gives the "cosine-like" behavior of the reduced Poincaré function.

Hypothesis **H3′** is trivially fulfilled thanks to the explicit form (48) for the function U^{k_0,l_0} and condition (10) on the Fourier coefficients. Finally, the last two hypotheses **H3″** and **H3‴** are sufficient conditions for the existence of transversal intersections between KAM tori close to resonances of the inner dynamics and their images under the scattering map. For the example in this paper, Eq. (59) guarantees the existence of these transversal intersections.

The paper is organized as follows: in Section 2 we introduce a representative a priori unstable Hamiltonian system with $2 + 1/2$ degrees of freedom and we state our main result: Theorem 2.1. It establishes the conditions for the existence of a diffusing orbit for the model considered. In Section 3 we perform the explicit verification of the geometric mechanism for the Hamiltonian of Theorem 2.1. The verification is structured in four parts, and includes a detailed description of the scattering map.

2. Set-up and main result

In [12] we gave explicit conditions for the existence of diffusing orbits for generic a priori unstable Hamiltonian systems. That paper was mainly focused on proving the genericity of the result, so although the conditions were explicit, some computational effort was required to check them. As we already mentioned in the introduction, in this paper we plan to give easily verifiable sufficient conditions, which guarantee the existence of diffusion for a representative type of a priori unstable Hamiltonian systems.

In this section, we first introduce a representative type of a priori unstable Hamiltonian systems of $2+1/2$ degrees of freedom, which is usually found with several variations in the literature [7, §7.5], [6, §9, §12], [4,2,3,26], when explicit computations are performed. Then, we discuss its features and particularities. Finally, we state Theorem 2.1, which establishes the existence of diffusing orbits under explicit and easily verifiable conditions.

We consider an a priori unstable Hamiltonian system as introduced by Chierchia and Gallavotti [6, Sections 7.5 and 12], consisting of a 2π-periodic in time perturbation of a pendulum and a rotor. It is given by the following non-autonomous Hamiltonian

$$\begin{aligned} H_\varepsilon(p,q,I,\varphi,t) &= H_0(p,q,I) + \varepsilon h(p,q,I,\varphi,t;\varepsilon) \\ &= P_\pm(p,q) + \frac{1}{2}I^2 + \varepsilon h(p,q,I,\varphi,t;\varepsilon). \end{aligned} \tag{1}$$

We notice that a motivation for the model above comes from a normal form around a resonance of a nearly integrable Hamiltonian, and we refer the reader to [10,22] for more details.

The second term $\frac{1}{2}I^2$ in the integrable Hamiltonian $H_0(p,q,I)$ of Hamiltonian (1) describes a *rotor* and the first one

$$P_\pm(p,q) = \pm\left(\frac{1}{2}p^2 + V(q)\right) \tag{2}$$

a *pendulum*. The potential $V(q)$ is a 2π-periodic function, whose non-degenerate maxima give rise to saddle points of the pendulum (2) and therefore, to hyperbolic invariant tori of the Hamiltonian (1) when $\varepsilon = 0$. Typically, it is assumed that the maximum of V is attained at the origin $q = 0$, where V is assumed to vanish. This is the case for the standard pendulum, where

$$V(q) = \cos q - 1. \tag{3}$$

This is the simple and standard choice of potential $V(q)$ that we are going to consider in this paper, so that

$$P_\pm(p,q) = \pm\left(\frac{p^2}{2} + \cos q - 1\right).$$

The origin ($p = 0$, $q = 0$) is a saddle point of the standard pendulum, and its *separatrix* $P_\pm^{-1}(0)$ for positive p is given by

$$q_0(t) = 4\arctan e^{\pm t}, \qquad p_0(t) = 2/\cosh t. \tag{4}$$

Notice that other choices of V give rise to different separatrices that are not usually so simple.

We also consider the negative sign in the pendulum (2) just to emphasize that the geometric mechanism we are using does not require the Hamiltonian H_0 to be positive definite, as it is the case in the variational approach, see for instance [9].

The term εh in (1) is the perturbation term and depends periodically on time and on the angular variable φ, so that h can be expressed via its Fourier series in the variables (φ, t) as

$$h(p,q,I,\varphi,t;\varepsilon) = \sum_{(k,l)\in\mathbb{Z}^2} h_{k,l}(p,q,I;\varepsilon)e^{\mathrm{i}(k\varphi+lt)}. \tag{5}$$

It is common in the literature (see the references at the beginning of this section) to consider a perturbation (5) depending only on the angular variables (q,φ,t), and formed by the product of a function of the pendulum variable q times a function of the angular variables (φ,t)

$$h(p,q,I,\varphi,t) = f(q)g(\varphi,t). \tag{6}$$

This is the kind of perturbation that we are going to consider along this paper, particularly because with this choice of h the Melnikov potential (15), which will be an essential tool for the computations along the paper, has the same harmonics as the function g, and they can be computed explicitly. So we will focus on a concrete type of Hamiltonians of the form

$$H_\varepsilon(p,q,I,\varphi,t) = \pm\left(\frac{p^2}{2}+\cos q-1\right)+\frac{I^2}{2}+\varepsilon f(q)g(\varphi,t), \tag{7}$$

defined for any real value of $(p,q,I,\varphi,t,\varepsilon)$ and 2π-periodic in the angular variables (q,φ,t).

The function f could be any 2π-periodic function. However, to easily compute the harmonics of the Melnikov potential (15), we are going to assume along this paper that f has the simple form:

$$f(q) = \cos q. \tag{8}$$

About the choice of f we would like to remark two important features. On the one hand, thanks to the fact that $f'(0)=0$, Hamiltonian (7) does not require the use of the theory of normally hyperbolic invariant manifolds (NHIM) to ensure the persistence of the NHIM defined later in (12). This simplifies the exposition and the computations, but since we do not assume $f(0)=0$ the problem maintains all the richness and complexity of the *large gap problem*. So, although the choice (8) for f may seem very restrictive, we would like to insist on the fact that the complexity of the more general a priori unstable Hamiltonian (1) is preserved. At the beginning of Section 3.1 we discuss in detail the role of the function f in the problem.

A general function g is of the form

$$g(\varphi,t) = \sum_{(k,l)\in\mathbb{N}^2} a_{k,l}\cos(k\varphi-lt-\sigma_{k,l}) + \tilde{a}_{k,l}\cos(k\varphi+lt-\tilde{\sigma}_{k,l}),$$

which in general has an *infinite number of harmonics* in the angles (φ,t) and where $\sigma_{k,l},\tilde{\sigma}_{k,l}\in\mathbb{T}$.

Since for simplicity we will study diffusion only for I positive along this paper, we will consider $\tilde{a}_{k,l}=0$, that is,

$$g(\varphi,t) = \sum_{(k,l)\in\mathbb{N}^2} a_{k,l}\cos(k\varphi-lt-\sigma_{k,l}). \tag{9}$$

In a natural way, and also for simplicity, we have chosen g to be an analytic function and therefore we will assume an exponential decay for its Fourier coefficients. That is, $|a_{k,l}|\leqslant e^{-\delta|(k,l)|}$, where δ is the size of the domain of analyticity. In this paper we simply are going to assume that they have some general lower bound with exponential decay, that is

$$e^{-\beta\delta|(k,l)|} \leqslant |a_{k,l}| \leqslant e^{-\delta|(k,l)|},$$

where $1 \leqslant \beta < 2$. Or, equivalently, we are going to assume

$$\hat{\alpha}\rho^{\beta k} r^{\beta l} \leqslant |a_{k,l}| \leqslant \alpha\rho^k r^l, \tag{10}$$

where $1 \leqslant \beta < 2$ and $0 < \hat{\alpha} < \alpha$. Moreover, $0 < \rho, r < 1$ are real numbers that will be chosen small enough.

The lower bound for the coefficients $a_{k,l}$ in the above equation may seem very restrictive, but there are several reasons for this particular choice. For the more expert reader, let us say that condition (10) implies that big gaps of maximal size appear for *all* the resonances in first order with respect to the parameter ε, without performing any step of averaging. This feature is explained thoroughly in Section 3.3, after Eq. (48). The second reason is that requirements (10) are simple to state and verify. A generic, and, of course, more technical, set of conditions for generic perturbations are given explicitly in [12]. When the lower bound condition for a_{kl} in (10) is not satisfied, several steps of averaging are needed to check the generic conditions of [12].

We can now state our main result:

Theorem 2.1. *Consider a Hamiltonian of the form* (7)*, where* $f(q)$ *is given by* (8) *and* $g(\varphi, t)$ *is any analytic function of the form* (9) *with non-vanishing Fourier coefficients satisfying* (10)*. Assume that*

$$\lambda := \left|\frac{a_{1,0}}{a_{0,1}}\right| < 1/1.6 \quad \text{or} \quad \lambda > 1.6, \tag{11}$$

as well as $0 < \rho \leqslant \rho^*$ *and* $0 < r \leqslant r^*$*, where* $\rho^*(\lambda, \alpha, \hat{\alpha}, \beta)$ *and* $r^*(\lambda, \alpha, \hat{\alpha}, \beta)$ *are small enough.*

Then, for any $I_+^* > 0$*, there exists* $\varepsilon^* = \varepsilon^*(I_+^*) > 0$ *such that for any* $-1/2 < I_- < I_+ \leqslant I_+^*$ *and* $0 < \varepsilon < \varepsilon^*$*, there exists a trajectory* $(p(t), q(t), I(t), \varphi(t))$ *of the Hamiltonian* (1) *such that for some* $T > 0$

$$I(0) \leqslant I_-; \qquad I(T) \geqslant I_+.$$

We want to remark now that not every perturbation (6) gives rise to diffusion in the action I. In particular, if the function $g(\varphi, t)$ in (9) does not depend on φ, the action I is a first integral, so it does not change at all. Moreover, if $g(\varphi, t)$ does not depend on t, Hamiltonian (7) is autonomous and therefore H_ε is a first integral, so that only deviations of size $\sqrt{\varepsilon}$ are possible for the action I. The same happens when the function $g(\varphi, t)$ does not depend fully on the two angular variables, but only through an integer linear combination of them—that is, $g(\varphi, t) = G(\psi)$, where $\psi = k_0\varphi - l_0 t$ is an integer combination of the angular variables (φ, t)—as can be easily checked by introducing ψ as a new angular variable. In these three cases, an infinite number of Fourier coefficients $a_{k,l}$ of the function $g(\varphi, t)$ in (9) vanish.

3. Proof of Theorem 2.1

In the following sections, we will consider any Hamiltonian satisfying the hypotheses of Theorem 2.1, and we will show how the geometric mechanism in [14,12] can be applied to construct diffusing orbits.

In the introduction of this paper we already mentioned that the geometric mechanism in [14,12] is based on the classical Arnold mechanism for diffusion. It consists of constructing a *transition chain*, that is, a finite sequence of transition tori such that the unstable manifold of each torus intersects transversally the stable manifold of the next one. As a main novelty, in [14,12] the transition chain incorporates primary as well as secondary KAM tori created by the *resonances* (as already mentioned in the introduction), in order to overcome the *large gap problem*.

In this paper, we will try to present a description of the mechanism that emphasizes more the geometric aspects. We think that this description may contribute to a better understanding and applicability of the mechanism.

To prove the existence of a diffusing orbit we will identify first an NHIM (normally hyperbolic invariant manifold) with associated stable and unstable manifolds. It will organize the different invariant objects involved in the transition chain (the skeleton for the diffusing orbit).

The diffusing orbit we are looking for starts on a point close to the NHIM and in finite time reaches another point close to the NHIM but arbitrarily far from the original one. Of course, if the starting point lies just on the 3-dimensional NHIM, the 2-dimensional invariant tori inside the NHIM act as barriers for diffusion and the orbit is confined in a bounded domain. Fortunately, there exists an external dynamics to the NHIM, provided by its associated stable and unstable manifolds, which will be essential to overcome the obstacles of the invariant tori and escape from them, as long as the starting point does not lie on the NHIM but very close to it. Hence, it is crucial for the mechanism that the external dynamics does not preserve the invariant tori existing in the NHIM. Otherwise, the orbit will be confined in a finite domain by both the inner and the outer dynamics with no possibility to escape.

Thus, given a Hamiltonian of the form (7), the outline of the proof of the existence of diffusing orbits has the following steps: Detect the 3-dimensional NHIM and the 4-dimensional associated stable and unstable manifolds, determine the inner and the outer dynamics of the NHIM as well as the invariant objects for each one, and finally show that the outer dynamics does not preserve the invariant objects for the inner one.

One of the novelties of this paper is the explicit description of the outer dynamics provided by the scattering map [15]. It is given by the ε time flow of a Hamiltonian that in first order is given by an autonomous Hamiltonian of one degree of freedom, therefore integrable. Moreover, using a geometric description, we obtain an explicit expression for this autonomous Hamiltonian, which is the reduced Poincaré function (39) with the opposite sign.

On the other hand, using averaging theory, one can show that the Hamiltonian defining the inner dynamics can be transformed into a normal form consisting of an integrable Hamiltonian plus a small perturbation.

Thus, we have two dynamics defined on the NHIM that can be approximated in suitable coordinates by one-degree of freedom autonomous Hamiltonians. The invariant objects are then given approximately by the level sets of these integrable Hamiltonians, for which we provide explicit expressions.

Finally, we impose that the outer dynamics moves the invariant tori of the inner dynamics, in such a way that the image under the outer dynamics of each of these invariant tori intersects transversally another torus.

3.1. Part 1. Existence of an NHIM and associated stable and unstable manifolds

The first part of the proof establishes the existence of an NHIM with associated stable and unstable manifolds that intersect transversally. To prove the existence of these invariant objects, we will compute them in the unperturbed case (where they can be obtained analytically) and then study their persistence under the perturbation.

For $\varepsilon = 0$, Hamiltonian H_0 in (7) consists of two uncoupled systems: a pendulum plus a rotor. Therefore, it is clear that the 3-dimensional manifold given by

$$\widetilde{\Lambda} = \left\{(0, 0, I, \varphi, s)\colon\ (I, \varphi, s) \in \mathbb{R} \times \mathbb{T}^2\right\} \tag{12}$$

is an invariant manifold with associated stable and unstable manifolds $W^s\widetilde{\Lambda}$, $W^u\widetilde{\Lambda}$ (inherited from the separatrices of the pendulum). These manifolds coincide along a separatrix given by

$$W^0\widetilde{\Lambda} = \left\{\big(p_0(\tau), q_0(\tau), I, \varphi, s\big)\colon\ \tau \in \mathbb{R},\ I \in \big[-1/2, I_+^*\big],\ (\varphi, s) \in \mathbb{T}^2\right\}, \tag{13}$$

where $(p_0(\tau), q_0(\tau))$ is the chosen orbit (4) of the pendulum, which is homoclinic to the saddle point $p = 0$, $q = 0$.

The integrable Hamiltonian H_0 has a one-parameter family of 2-dimensional whiskered tori given by

$$\mathcal{T}_I^0 = \big\{(0, 0, I, \varphi, s)\colon (\varphi, s) \in \mathbb{T}^2\big\}, \tag{14}$$

with associated frequency $(I, 1)$.

When we consider the perturbation h, that is $\varepsilon > 0$, using the standard theory of NHIM, see [21,17], we know that for $\varepsilon > 0$ small enough, the manifold $\widetilde{\Lambda}$ persists, as well as its local stable and unstable manifolds.

Nevertheless, for any general perturbation h of the form (6), if $f'(0) = 0$, the NHIM is preserved without any deformation for any ε: $\widetilde{\Lambda}_\varepsilon = \widetilde{\Lambda}$, because $p = q = 0 \Rightarrow \dot{p} = \dot{q} = 0$. Moreover, if $f(0) = 0$, the perturbation vanishes on $\widetilde{\Lambda}$, so the one-parameter family of 2-dimensional invariant tori existing in the unperturbed case remains fixed under the perturbation, as in the Arnold's example of diffusion in [1]. However, a generic perturbation $f(0) \neq 0$, creates gaps of size $\sqrt{\varepsilon}$ in the foliation of persisting invariant tori and gives rise to the *large gap problem*. See Section 3.3 for a detailed description of the invariant objects in this foliation.

Although it is not a generic assumption, for the clarity of exposition and for the convenience of the reader not familiar with the theory of NHIM, we have chosen in Theorem 2.1 a function f in (8) so that the NHIM is preserved without deformation, that is $f'(0) = 0$. Nevertheless, we want to emphasize that this is not a necessary hypothesis for the existence of diffusion. Indeed this was not assumed in the proof of the result in [14,12] where NHIM theory was used. Of course, any other function f satisfying the conditions $f'(0) = 0$ and $f(0) \neq 0$ will be enough for exhibiting the *large gap problem*, but we have chosen the *concrete* one (8) so that the Fourier coefficients for the Melnikov potential (15) can be computed *explicitly*.

Even if for the function f in (8) the NHIM remains fixed, when the local stable and unstable manifolds are extended to global ones it is expected that, in general, they will no longer coincide and indeed they will intersect transversally along a homoclinic manifold. The main tool to study the splitting of the separatrix (13) as well as the associated scattering map is the *Melnikov potential* associated to a perturbation h and to the homoclinic orbit (p_0, q_0):

$$\begin{aligned}\mathcal{L}(I, \varphi, s) = -\int_{-\infty}^{+\infty} \big(&h\big(p_0(\sigma), q_0(\sigma), I, \varphi + I\sigma, s + \sigma; 0\big) \\ &- h(0, 0, I, \varphi + I\sigma, s + \sigma; 0)\big)\, d\sigma,\end{aligned} \tag{15}$$

which taking into account the expression (6) for h, takes the form

$$\mathcal{L}(I, \varphi, s) = \int_{-\infty}^{\infty} \big[f\big(q_0(\sigma)\big) - f(0)\big] g(\varphi + I\sigma, s + \sigma)\, d\sigma. \tag{16}$$

Notice that by the expression (4) of $q_0(t)$, the improper integrals (15) and (16) are exponentially convergent.

In our concrete case $f(q) = \cos q$ of (8), the Melnikov potential turns out to be

$$\mathcal{L}(I, \varphi, s) = \frac{1}{2} \int_{-\infty}^{\infty} p_0^2(\sigma) g(\varphi + I\sigma, s + \sigma)\, d\sigma,$$

and the integral can be explicitly computed by the residue theorem:

$$\mathcal{L}(I,\varphi,s)=\sum_{(k,l)\in\mathbb{N}^2} A_{k,l}(I)\cos(k\varphi-ls-\sigma_{k,l}), \tag{17}$$

with

$$A_{k,l}(I)=2\pi\,\frac{(kI-l)}{\sinh\frac{\pi}{2}(kI-l)}a_{k,l}, \tag{18}$$

where $a_{k,l}$ are the general coefficients of the function g given in (9). Notice that the Melnikov potential (17) has exactly the same harmonics as the perturbation g in (9).

The role played by the Melnikov potential in the splitting of the separatrix (13) is summarized in the following proposition (which is a short version of Proposition 9.2 in [14]; recall that $\widetilde{\Lambda}_\varepsilon=\widetilde{\Lambda}$ in this paper by the hypotheses of Theorem 2.1):

Proposition 3.1. *Given $(I,\varphi,s)\in[-1/2,I_+^*]\times\mathbb{T}^2$, assume that the function*

$$\tau\in\mathbb{R}\mapsto\mathcal{L}(I,\varphi-I\tau,s-\tau) \tag{19}$$

has a non-degenerate critical point $\tau^*=\tau^*(I,\varphi,s)$. (By the implicit function theorem, the function τ^* is smooth.)

Then, for $\varepsilon>0$ small enough there exists a locally unique transversal homoclinic point z to $\widetilde{\Lambda}_\varepsilon$ which is ε-close to the point $z^*(I,\varphi,s)=(p_0(\tau^*),q_0(\tau^*),I,\varphi,s)$ of the unperturbed separatrix $W^0\widetilde{\Lambda}$ given in (13):

$$z=z(I,\varphi,s;\varepsilon)=\big(p_0\big(\tau^*\big),q_0\big(\tau^*\big),I,\varphi,s\big)+\mathcal{O}(\varepsilon)\in W^s(\widetilde{\Lambda}_\varepsilon)\pitchfork W^u(\widetilde{\Lambda}_\varepsilon). \tag{20}$$

Next, we are going to find open sets of $(I,\varphi,s)\in[-1/2,I_+^*]\times\mathbb{T}^2$, such that the function (19) has non-degenerate critical points at $\tau=\tau^*(I,\varphi,s)$.

Taking into account the explicit expression for the Melnikov potential (17), the function (19) takes the form

$$\mathcal{L}(I,\varphi-I\tau,s-\tau)=\sum_{(k,l)\in\mathbb{N}^2} A_{k,l}(I)\cos\big(k\varphi-ls-\tau(kI-l)\big), \tag{21}$$

with $A_{k,l}(I)$ as in (18). Notice that the Fourier coefficients $A_{k,l}(I)$ are nothing else but the Fourier coefficients $a_{k,l}$ multiplied by a non-zero factor depending on $kI-l$ (which decreases exponentially in $|kI-l|$ as $|kI-l|$ goes to infinity).

The main reason for the introduction of the upper bounds for $|a_{k,l}|$ in (10) is to make all the computations for the series defining $\mathcal{L}(I,\varphi,s)$ in (17) and (21) in terms of $\mathcal{L}^{[\leqslant 1]}(I,\varphi,s)$, its first order trigonometric polynomial in the angles (φ,s). Thus, we have

$$\begin{aligned}\mathcal{L}(I,\varphi,s) &= A_{0,0}+A_{1,0}(I)\cos\varphi+A_{0,1}\cos s+\mathcal{O}_2(\rho,r)\\ &:=\mathcal{L}^{[\leqslant 1]}(I,\varphi,s)+\mathcal{L}^{[>1]}(I,\varphi,s),\end{aligned} \tag{22}$$

where $A_{0,0}=4a_{0,0}$,

$$A_{0,1}=\frac{2\pi}{\sinh(\pi/2)}a_{0,1}\quad\text{and}\quad A_{1,0}(I)=\frac{2\pi I}{\sinh(\pi I/2)}a_{1,0}. \tag{23}$$

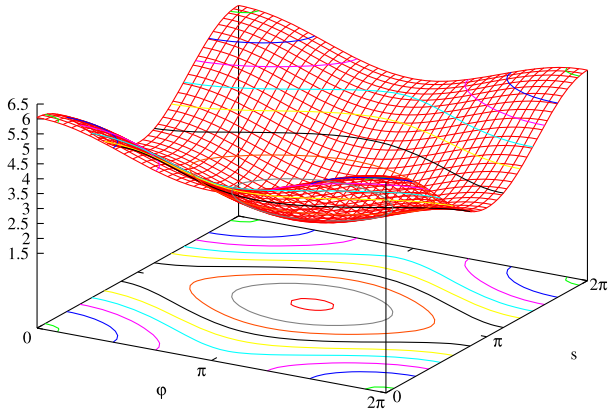

Fig. 1. Graph and level curves of the Melnikov potential $\mathcal{L}^{[\leqslant 1]}(I,\varphi,s)$ with $a_{1,0}=1/4$, $a_{0,1}=1/2$ and $I=1$. In this case, $A_{0,0}=4$, $A_{1,0}(1)=\pi/(2\sinh(\pi/2))$ and $A_{0,1}=\pi/\sinh(\pi/2)$.

In the formula above, without loss of generality and to avoid cumbersome notation and shifts in the pictures, we have assumed that $\sigma_{1,0}=\sigma_{0,1}=0$. Otherwise, we can just make a translation in the variables (φ,s).

Next we will make our computations for the function $\mathcal{L}^{[\leqslant 1]}$ and a posteriori we will justify that they are also valid for the complete function $\mathcal{L}$.

So fixing $(I,\varphi,s)\in[-1/2,I_+^*]\times\mathbb{T}^2$ we only need to study the evolution of $\mathcal{L}^{[\leqslant 1]}$ along the straight lines

$$R=R(I,\varphi,s):\quad \tau\in\mathbb{R}\mapsto(\varphi-I\tau,s-\tau)\in\mathbb{T}^2 \tag{24}$$

on the torus.

By hypothesis (10), $a_{1,0}\neq 0$ and $a_{0,1}\neq 0$, and therefore $|A_{0,1}|\neq 0$ and $|A_{1,0}(I)|\neq 0$ for any I. Consequently, for every fixed I, the first order trigonometric polynomial $(\varphi,s)\mapsto\mathcal{L}^{[\leqslant 1]}(I,\varphi,s)$ possesses in $\mathbb{T}^2$ four non-degenerate critical points at $(0,0)$, $(0,\pi)$, $(\pi,0)$ and (π,π); a maximum, a minimum and two saddle points, respectively. Without loss of generality and for illustration purposes we will assume from now on that $a_{1,0}>0$ and $a_{0,1}>0$, so that $A_{1,0}(I)>0$ and $A_{0,1}>0$ for any I. In this way the maximum of $\mathcal{L}^{[\leqslant 1]}(I,\cdot,\cdot)$ is attained at $(0,0)$, the minimum at (π,π) and the two saddles at $(0,\pi)$ and $(\pi,0)$ (see Fig. 1). Of course, assuming that $0<\rho\leqslant\rho^*$ and $0<r\leqslant r^*$, for ρ^* and r^* small enough, by the implicit function theorem, the function $\mathcal{L}(I,\cdot,\cdot)$ possesses also exactly four non-degenerate critical points close to ones of $\mathcal{L}^{[\leqslant 1]}(I,\cdot,\cdot)$, with the same properties.

Around the two extremum points (the maximum and the minimum), the level curves of the function $\mathcal{L}(I,\cdot,\cdot)$ are closed curves which fill out a region bounded by the level curve containing one of the two saddle points (the saddle point $(\pi,0)$ for the maximum and $(0,\pi)$ for the minimum). We will call these regions *extremum basins*, and we will distinguish between the maximum and minimum basin. Notice that any time that the straight line (24) enters into one of the two extremum basins, it is tangent to one of the closed level curves of this extremum basin, giving rise to one extremum of (19). Since the two extrema of $\mathcal{L}(I,\cdot,\cdot)$ are non-degenerate for any I, the closed level curves close to the extrema are convex. Thus, every time that the straight line (24) passes close enough to one extremum of $\mathcal{L}(I,\cdot,\cdot)$, it gives rise to a locally unique non-degenerate extremum of (19). In particular, for irrational values of I, the line (24) is a dense straight line in the torus $\{(\varphi,s)\}$, so that there exist an infinite number of non-degenerate extrema for (19). Thanks to the form of the perturbation in Theorem 2.1, we are going to see that indeed *all* the closed level curves in any of the two extremum basins are convex, so every time that a straight line (24) enters some extremum basin, it gives rise to a non-degenerate extremum of the function (19).

To do so, we proceed in the following way. Given a fixed value of I, let us look for the geometric locus where the straight lines (24) are tangent to the level curves of $\mathcal{L}(I,\cdot,\cdot)$. The tangency is equivalent to saying that $\nabla_{\varphi,s}\mathcal{L}$, the gradient of $\mathcal{L}(I,\cdot,\cdot)$, is orthogonal to the slope $(I,1)$ of the straight line (24):

$$I\frac{\partial \mathcal{L}}{\partial \varphi}(I,\varphi,s)+\frac{\partial \mathcal{L}}{\partial s}(I,\varphi,s)=0. \tag{25}$$

Intuitively, for fixed I, if we want to pass through a mountain of height $\mathcal{L}(I,\varphi,s)$ along straight lines following a direction $(I,1)$, Eq. (25) gives the position of the points (φ,s) of maximum height, the *crest*, that we will denote along this paper by $\mathcal{C}=\mathcal{C}(I)$. We will also use the notation $\mathcal{C}$ for the sets satisfying (25) for the case of a minimum, although this may seem counterintuitive.

Using expression (22) for $\mathcal{L}$, Eq. (25) has the form

$$IA_{1,0}(I)\sin\varphi+A_{0,1}\sin s+\mathcal{O}_2(\rho,r)=0.$$

Disregarding first the $\mathcal{O}_2(\rho,r)$ term we are faced with the following implicit equation

$$\alpha(I)\sin\varphi+\sin s=0, \tag{26}$$

where

$$\alpha(I):=\frac{IA_{1,0}(I)}{A_{0,1}}=\frac{\sinh(\pi/2)I^2}{\sinh(\pi/2I)}\frac{a_{1,0}}{a_{0,1}}. \tag{27}$$

Assuming that

$$\big|\alpha(I)\big|<1,$$

which holds for all I as long as

$$1.03\left|\frac{a_{1,0}}{a_{0,1}}\right|<1, \tag{28}$$

and that ρ and r are small enough, Eq. (25) defines exactly two closed curves $\mathcal{C}_M$ and $\mathcal{C}_m$, parameterized by φ, which will be called *crests*. The crest $\mathcal{C}_M=\mathcal{C}_M(I)$, passing through the maximum $(0,0)$ of $\mathcal{L}$, contains the saddle $(0,\pi)$ and is given by $s=\xi_M(\varphi,I)\pmod{2\pi}$, where

$$\xi_M(\varphi,I)=-\arcsin\big(\alpha(I)\sin\varphi\big)+\mathcal{O}_2(\rho,r). \tag{29}$$

The crest $\mathcal{C}_m=\mathcal{C}_m(I)$, passing through the minimum (π,π) of $\mathcal{L}$, contains the saddle $(\pi,0)$ and is given by $s=\xi_m(\varphi,I)\pmod{2\pi}$, where

$$\xi_m(\varphi,I)=\arcsin\big(\alpha(I)\sin\varphi\big)+\pi+\mathcal{O}_2(\rho,r). \tag{30}$$

In Fig. 2 there appear these two curves (dashed black) as well as the level sets of the function $\mathcal{L}^{[\leqslant 1]}$.

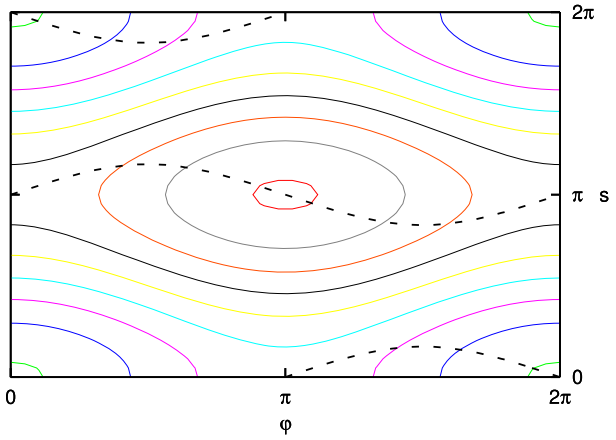

Fig. 2. Closed curves satisfying (26) for $I = 1$ (the crests), dashed black, and level sets of the function $\mathcal{L}^{[\leqslant 1]}(1,\cdot,\cdot)$ with the same values as in Fig. 1.

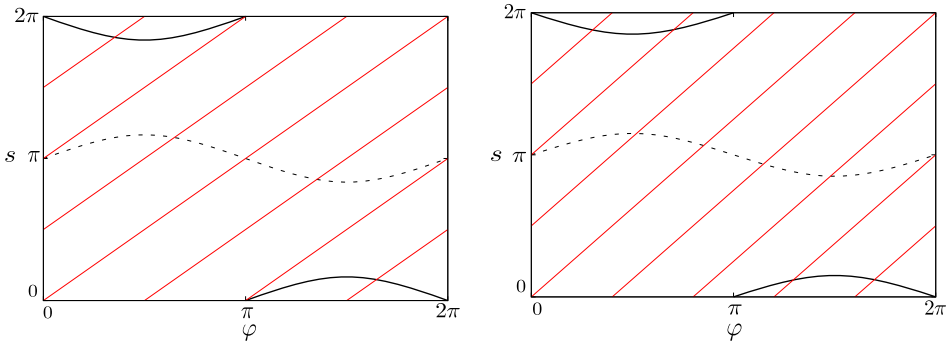

Fig. 3. Straight lines (24) with slope 1 (left) and 0.8 (right) and the curves (26): the curve of the maxima (solid curve) and the curve of the minima (dashed curve). See the text.

Remark 3.2. The case $|\alpha(I)| > 1$ is totally analogous to $|\alpha(I) < 1|$, but exchanging the roles of φ and s. The case $|\alpha(I)| = 1$ is special because the union of the two curves, $\mathcal{C}_m$ and $\mathcal{C}_M$, degenerates into two straight lines along which the function $\mathcal{L}$ is constant.

The special case $|\alpha(I)| = 1$ will not be considered in this paper. We will only consider both the cases $|\alpha(I)| < 1$ and $|\alpha(I)| > 1$, but we will only work out the details for the first one, since the second is identical exchanging φ and s.

For any point $(I, \varphi, s) \in [-1/2, I_+^*] \times \mathbb{T}^2$, the real values τ^* for which the function (19) has a non-degenerate critical point satisfy $(\varphi - I\tau^*, s - \tau^*) \in \mathcal{C}_m(I) \cup \mathcal{C}_M(I)$. We state now this geometrical feature.

Proposition 3.3. *Assuming $|a_{1,0}/a_{0,1}| < 1/1.03$ or $|a_{1,0}/a_{0,1}| > 1/1.03$, for any point $(I, \varphi, s) \in [-1/2, I_+^*] \times \mathbb{T}^2$, the non-degenerate critical points $\tau^*(I, \varphi, s)$ of* (19) *are achieved at the intersection of the straight line* (24) *with either the crest $\mathcal{C}_M$ or $\mathcal{C}_m$.*

Of course, for any point (I, φ, s) there exist several intersections of the line (24) with the crests $\mathcal{C}_M$ and $\mathcal{C}_m$, parameterized by several values τ^* of the parameter τ. See Fig. 3. According to Proposition 3.1, each one of the transversal intersections of the line (24) with the crests gives rise, for

$\varepsilon > 0$ small enough, to a transversal homoclinic point $z(I,\varphi,s,\varepsilon)$ of $\widetilde{\Lambda}$ which is ε-close to the point $z^*(I,\varphi,s)$ of the unperturbed separatrix $W^0\widetilde{\Lambda}$. Fixed (I,φ,s), notice that for a rational value of I, the number of generated homoclinic points $z(I,\varphi,s,\varepsilon)$ is finite, whereas for irrational I is arbitrarily large.

From now on, we choose only one of these intersections, the "first one" with the crest $\mathcal{C}_M$. Given (I,φ,s), we define $\tau^*(I,\varphi,s) = \tau^*_M(I,\varphi,s)$ as the real number τ with minimum absolute value $|\tau|$ among all τ satisfying

$$(\varphi - I\tau, s - \tau) \in \mathcal{C}_M(I).$$

In symbols, $\tau^*(I,\varphi,s) \in \mathcal{T}_M(I,\varphi,s)$ is such that

$$\forall \tau \in \mathcal{T}_M(I,\varphi,s), \quad \tau \neq \tau^*(I,\varphi,s) \quad \Rightarrow \quad |\tau| > \left|\tau^*(I,\varphi,s)\right|, \tag{31}$$

where

$$\mathcal{T}_M(I,\varphi,s) = \left\{\tau \in \mathbb{R}\colon\ (\varphi - I\tau, s - \tau) \in \mathcal{C}_M(I)\right\}.$$

To determine a domain of definition as large as possible in the variables (I,φ,s) where the function $\tau^*(I,\varphi,s)$ defined in (31) is well defined and continuous and to avoid a casuistic discussion, it suffices to check that for any fixed I, the straight lines cross only once the crest $\mathcal{C}_M$ inside the domain (φ,s) and they do it transversally. This implies that for any fixed I, the slope $1/I$ of the straight lines is bigger than the slope of the derivative of the function $\xi_M(\varphi,I)$ for all $\varphi \in \mathbb{T}$, that is

$$\frac{1}{I} > \frac{\partial \xi_M}{\partial \varphi}(\varphi, I), \quad \text{for all } \varphi \in \mathbb{T}, \tag{32}$$

which by Eqs. (29) and (27) and assuming that ρ and r are small enough, is equivalent to

$$\alpha(I) I < 1.$$

By expression (27) for $\alpha(I)$, it is easy to see that

$$\alpha(I) I < 1.6 \frac{a_{1,0}}{a_{0,1}},$$

so that condition (32) holds for all I as long as

$$1.6 \left|\frac{a_{1,0}}{a_{0,1}}\right| < 1, \tag{33}$$

which is exactly hypotheses (11) of Theorem 2.1 and implies (28).

Under condition (33), one suitable maximal domain of definition $H = H_M$ containing the crests $\mathcal{C}_M(I)$, where τ^* is continuous, consists of excluding, for any $I \in [-1/2, I^*_+]$, the crest $\mathcal{C}_m(I)$ from the domain of (φ,s), that is

$$\begin{aligned} H &= \left\{(I,\varphi,s) \in \left[-1/2, I^*_+\right] \times \mathbb{T} \times \mathbb{T}\colon\ (\varphi,s) \notin \mathcal{C}_m(I)\right\} \\ &= \left\{(I,\varphi,s) \in \left[-1/2, I^*_+\right] \times \mathbb{T} \times \mathbb{T}\colon\ s \neq \xi_m(I,\varphi) \ (\mathrm{mod}\ 2\pi)\right\}. \end{aligned} \tag{34}$$

See Fig. 4.

Remark 3.4. In a complete analogous way to definition (31), we could have chosen $\tau^*(I,\varphi,s) = \tau_m^*(I,\varphi,s)$ as the "first" intersection of the line (24) with the crest $\mathcal{C}_m$. Under the same condition (33), we can define $H = H_m$ analogously to (34) as a maximal open domain containing the crests $\mathcal{C}_m(I)$ where $\tau_m^*(I,\varphi,s)$ is continuous. These two "first" intersections give rise to homoclinic manifolds to $\widetilde{\Lambda}$ that are commonly named as *primary homoclinic* in the literature, since they exist for all the values of the perturbation parameter ε once assumed small enough, and they tend to unperturbed homoclinic orbits as ε tends to 0. For simpler NHIM like equilibrium points or periodic orbits, see, for instance, [25,5] for this terminology of primary homoclinic orbits.

We can now apply Proposition 3.1 to prove the existence of a primary homoclinic manifold Γ_ε. We have shown that if condition (11) is satisfied, for any (I,φ,s) in the domain H defined in (34) the function (19) has a non-degenerate critical point τ^* given by $\tau^* = \tau^*(I,\varphi,s)$, where τ^* is a smooth function defined in (31). By Proposition 3.1, if $0 < \varepsilon < \varepsilon^*(I_+^*)$, the critical points $\tau^*(I,\varphi,s)$ give rise to a homoclinic manifold $\Gamma_\varepsilon \subset W^s\widetilde{\Lambda} \pitchfork W^u\widetilde{\Lambda}$, along which the invariant manifolds intersect transversally. By Eq. (20), it has the form

$$\Gamma_\varepsilon = \left\{ z = z(I,\varphi,s;\varepsilon) = \left(p_0\left(\tau^*\right), q_0\left(\tau^*\right), I, \varphi, s\right) + \mathcal{O}(\varepsilon)\colon\ (I,\varphi,s) \in H,\ \tau^* = \tau^*(I,\varphi,s) \in \mathbb{R} \right\}. \quad (35)$$

Remark 3.5. For the experts in the splitting of separatrices, we notice that the size of ε^* required for the justification of the transversal intersection of $W^s\widetilde{\Lambda}$ and $W^u\widetilde{\Lambda}$ along Γ_ε has to be such that the Melnikov potential (17) gives the dominant part of the formula for the splitting. In our case, since $\mathcal{L}$ as well as its two first derivatives are $\mathcal{O}(\exp(-\pi/2I_+^*))$ on the domain H, we need to impose that $\varepsilon^* = \mathcal{O}(\exp(-\pi/2I_+^*))$.

Remark 3.6. Condition (33), or more generally condition (11), is very convenient since it provides a large domain of definition H for τ^*, and therefore it allows us to define a global homoclinic manifold Γ_ε. Although condition (11) imposes some restrictions on the perturbation h of Theorem 2.1, it is not necessary for the mechanism of diffusion. Indeed, if condition (11) is not satisfied we can obtain several homoclinic manifolds giving rise to different scattering maps, offering more possibilities for diffusion. It also opens the field for studying homoclinic bifurcations for an NHIM (see [16]).

Remark 3.7. For fixed I, the crest $\mathcal{C}_M = \mathcal{C}_M(I)$ is in the maximum basin of $\mathcal{L}(I,\cdot,\cdot)$, so the function $\mathcal{L}(I,\cdot,\cdot)$ decreases when one travels from $(\varphi,s) = (0,0)$ to $(\pi,0)$ increasing φ along the curve $\mathcal{C}_M$, and increases when one travels from $(\varphi,s) = (\pi,0)$ to $(2\pi,0)$. Analogously, the other crest $\mathcal{C}_m$ is in the minimum basin of $\mathcal{L}(I,\cdot,\cdot)$ with the opposite property. Since by (25) and (32), the curve $(\varphi,\xi_M(I,\varphi))$ is never tangent to the level sets of the function $\mathcal{L}(I,\cdot,\cdot)$, these increases and decreases are *strict*.

3.2. Part 2. Outer dynamics (scattering map)

In the previous section we have proved the existence of an NHIM $\widetilde{\Lambda}$ given in (12) with associated stable and unstable manifolds, $W^s\widetilde{\Lambda}$ and $W^u\widetilde{\Lambda}$, which intersect transversally along a homoclinic manifold Γ_ε given in (35).

Associated to the homoclinic manifold Γ_ε we can define an outer dynamics S_ε to the NHIM $\widetilde{\Lambda}$ and we will obtain an approximate explicit expression for it.

The scattering map associated to Γ_ε is defined in a domain H_ε contained in the domain H of definition of the function τ^* given in (34), in the following way:

$$\begin{aligned} S_\varepsilon : H_\varepsilon \subset H \subset \widetilde{\Lambda} &\to \widetilde{\Lambda}, \\ x_- &\mapsto x_+ \end{aligned} \quad (36)$$

such that $x_+ = S_\varepsilon(x_-)$ if and only if there exists $z \in \Gamma_\varepsilon$ such that

$$\operatorname{dist}\big(\Phi_{t,\varepsilon}(z), \Phi_{t,\varepsilon}(x_\pm)\big) \to 0 \quad \text{for } t \to \pm\infty,$$

where $\Phi_{t,\varepsilon}$ is the flow of the Hamiltonian (7).

In words, the scattering map maps a point x_- on the NHIM to a point x_+ on the NHIM if there exists a homoclinic orbit to the NHIM that approaches the orbit of x_- in the past and the orbit of x_+ in the future.

The scattering map S_ε is exact and symplectic and indeed it is Hamiltonian. It is given by the time ε map of a Hamiltonian $\mathcal{S}_\varepsilon$ [15]. In the variables (I, φ, s) this implies that the following formula holds for the scattering map

$$S_\varepsilon(I, \varphi, s) = \left(I - \varepsilon \frac{\partial \mathcal{S}_0}{\partial \varphi}(I, \varphi, s) + \mathcal{O}\big(\varepsilon^2\big), \varphi + \frac{\partial \mathcal{S}_0}{\partial I}(I, \varphi, s) + \mathcal{O}\big(\varepsilon^2\big), s \right). \tag{37}$$

Notice that the variable s is preserved by the scattering map. As it is described in Eq. (21) in [12], relying on the result in [15], the dominant term $\mathcal{S}_0$ of the Hamiltonian is given by

$$\mathcal{S}_0(I, \varphi, s) = -\mathcal{L}^*(I, \theta), \qquad \theta = \varphi - Is, \tag{38}$$

where $\mathcal{L}^*(I, \theta)$ is the *reduced Poincaré function* defined implicitly by

$$\mathcal{L}^*(I, \varphi - Is) := \mathcal{L}\big(I, \varphi - I\tau^*(I, \varphi, s), s - \tau^*(I, \varphi, s)\big), \tag{39}$$

or explicitly by

$$\mathcal{L}^*(I, \varphi) := \mathcal{L}\big(I, \varphi - I\tau^*(I, \varphi, 0), -\tau^*(I, \varphi, 0)\big). \tag{40}$$

It is important to notice that in the variables $I, \theta = \varphi - Is$, the Hamiltonian $\mathcal{S}_0$ is indeed an autonomous one-degree of freedom Hamiltonian, $-\mathcal{L}^*(I, \theta)$, so that in these variables (I, θ, s), the scattering map reads as

$$S_\varepsilon(I, \theta, s) = \left(I + \varepsilon \frac{\partial \mathcal{L}^*}{\partial \theta}(I, \theta) + \mathcal{O}\big(\varepsilon^2\big), \theta - \varepsilon \frac{\partial \mathcal{L}^*}{\partial I}(I, \theta) + \mathcal{O}\big(\varepsilon^2\big), s \right), \tag{41}$$

and the iterates under the scattering map simply follow closely the level curves of the reduced Poincaré function (39). Notice that the variable s is preserved by the scattering map, so it simply plays the role of a parameter. Notice also that up to first order in ε, the scattering map (37) is defined on H, although it can take values outside of H for points $(I, \varphi - Is)$ which are ε-close to the boundary $\bigcup_{\{I\} \in [-1/2, I_+^*]} I \times \mathcal{C}_m(I)$ of H. A simple way to have the scattering map (41) expressed in variables (I, θ, s) in a domain D and with values in D under successive iterates, consists of restricting the variable s to a bounded size so that it satisfies $|s| < \arcsin|\alpha(I)|$ (see formula (30)). Take, for instance,

$$D = \big\{ (I, \theta, s) \in \big[-1/2, I_+^*\big] \times \mathbb{T} \times \mathbb{T} \colon |s| < \pi/2 \ (\operatorname{mod} 2\pi) \big\}, \tag{42}$$

which is the domain for the scattering map (41) that we are going to consider from now on.

Remark 3.8. We restrict the domain D in the s variable because the restricted Poincaré function has monodromy with respect to the variable s. Indeed, non-trivial loops in this variable give rise to a multi-valued reduced Poincaré function. On the other hand, non-trivial loops in the variable θ or φ are allowed in the domain D because the function is 2π-periodic in these variables, and therefore, single-valued.

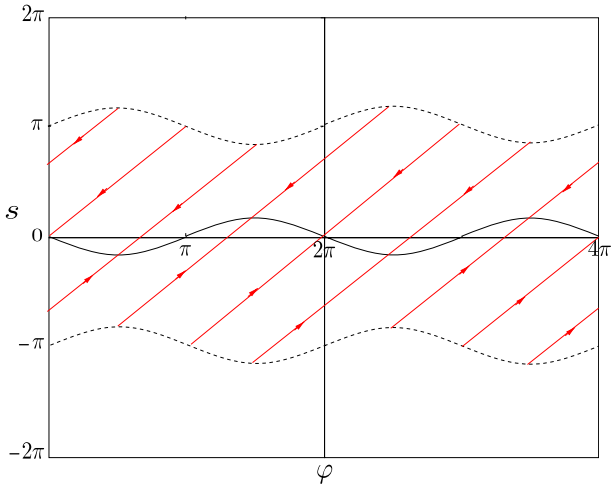

Fig. 4. Straight lines (24) with slope 1 and the curves (26): the curve of the maxima (solid curve) and the curve of the minima (dashed curve). See the text.

Although the variable $\theta = \varphi - Is$ is not a variable on the torus, that is, it is not defined $\pmod{2\pi}$ for arbitrary I and s $\pmod{2\pi}$, the variable θ parameterizes the crest $\mathcal{C}_M$, so it is 2π-periodic along it. We are going to check now that the crest $\mathcal{C}_M(I)$ is a natural domain of definition of the reduced Poincaré function $\mathcal{L}^*$, see (40), so the first approximation in ε in expression (41) is well defined in terms of θ.

In order to obtain an expression for the reduced Poincaré function and for its level curves in our particular example, we will perform a discussion based on geometric considerations.

By the definition of $\tau^*(I, \varphi, s)$ given in the previous section we have that the point

$$c(I, \varphi, s) := \big(\varphi - I\tau^*(I, \varphi, s), s - \tau^*(I, \varphi, s)\big) \in \mathcal{C}_M(I), \tag{43}$$

belongs to the crest $\mathcal{C}_M$, which is the closed curve defined in (29).

Therefore, the reduced Poincaré function $\mathcal{L}^*$ evaluated on a point (I, φ, s) in the domain H defined in (34) provides the value of the function $\mathcal{L}$ evaluated on $(I, c(I, \varphi, s))$, the closest intersection of the straight line (24) starting on this point (I, φ, s) with the curve $\mathcal{C}_M$. By construction, it is clear that any segment of points (I, φ, s) of the straight line (24) in the domain H gives rise to the same $c(I, \varphi, s)$ on the curve $\mathcal{C}_M$. See Fig. 4.

Since the function $\mathcal{L}^*$ is constant on these segments it can be written as a function of only two variables: the action I and the variable $\theta = \varphi - Is$, which is 2π-periodic in φ and constant along the straight lines (24) of slope $1/I$ contained in (34).

By Eq. (40), the function $\mathcal{L}^*$ has the following expression:

$$\mathcal{L}^*(I, \theta) = \mathcal{L}\big(I, \theta - I\tau^*(I, \theta, 0), -\tau^*(I, \theta, 0)\big). \tag{44}$$

The behavior of the function $\mathcal{L}^*$ with respect to the variable θ (which parameterizes the curve $\mathcal{C}_M$) is exactly the behavior of the function $\mathcal{L}$ along the curve $\mathcal{C}_M$, that we already discussed in Remark 3.7. Namely, when θ increases from 0 to π, one travels from $(\varphi, s) = (0, 0)$ to $(\pi, 0)$ increasing φ along the curve $\mathcal{C}_M$, and therefore the function $\mathcal{L}^*$ decreases strictly. Equivalently, when θ increases from π to 2π, one travels from $(\varphi, s) = (\pi, 0)$ to $(2\pi, 0)$ increasing φ along the curve $\mathcal{C}_M$, and therefore the function $\mathcal{L}^*$ increases strictly.

We summarize some of the properties of the reduced Poincaré function in the following proposition:

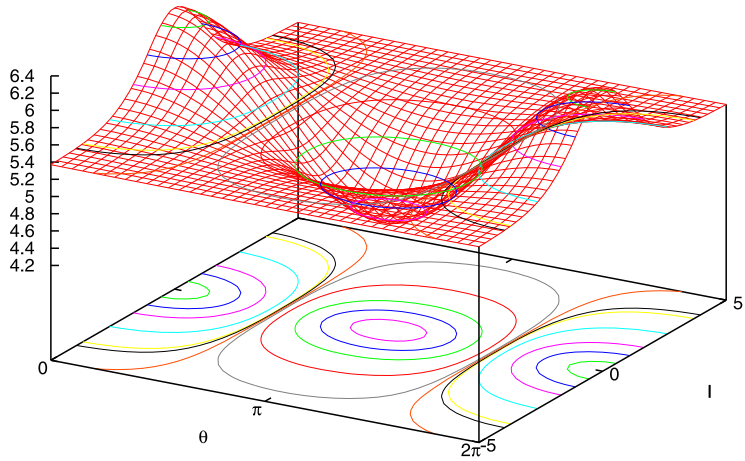

Fig. 5. Graph and level curves of the reduced Poincaré function $\mathcal{L}^*(I,\theta)$ given in (45). As in Fig. 1 we have chosen $a_{1,0}=1/4$ and $a_{0,1}=1/2$ in (23).

Proposition 3.9. *For any $I\in[-1/2,I_+^*]$, the function $\theta\mapsto\mathcal{L}^*(I,\theta)$ has a non-degenerate maximum (minimum) close to $\theta=0 \pmod{2\pi}$ ($\theta=\pi \pmod{2\pi}$, respectively) and is strictly monotone in all the other points θ. Moreover, it has the following expression*

$$\mathcal{L}^*(I,\theta)=A_{0,0}+A_{1,0}(I)\cos\big(\theta-I\tau^*(I,\theta,0)\big)+A_{0,1}\cos\big(\xi_M\big(I,\theta-I\tau^*(I,\theta,0)\big)\big)+\mathcal{O}_2(\rho,r), \tag{45}$$

where $A_{1,0}$ and $A_{0,1}(I)$ are given in (23)*, ξ_M in* (29) *and $\tau^*(I,\theta,0)$ is defined in* (31)*.*

Remark 3.10. Notice that the behavior of the function $\mathcal{L}^*$ with respect to the variable θ is "cosine-like". This observation is clear when one considers the case $I=0$, where $\varphi=\theta$, $\xi_M(0,\varphi)=0$ and

$$\mathcal{L}^*(0,\theta)=A_{0,0}+A_{1,0}(0)\cos(\theta)+A_{0,1}+\mathcal{O}_2(\rho,r).$$

Proposition 3.9 provides us with an exhaustive description of the level sets of the reduced Poincaré function, giving an approximate expression in first order for the orbits of the scattering map S_ε in (41). In Fig. 5 we illustrate these level curves for a particular case.

3.3. Part 3. Inner dynamics

The inner dynamics is the dynamics of the flow of Hamiltonian (7) restricted to the NHIM $\widetilde{\Lambda}$ defined in (12). Indeed, by the form of the perturbation, the Hamiltonian restricted to the NHIM takes the explicit form

$$K(I,\varphi,s;\varepsilon)=\frac{I^2}{2}+\varepsilon g(\varphi,s), \tag{46}$$

where $(I,\varphi,s)\in[-1/2,I_+^*]\times\mathbb{T}^2$ and g is given in (9).

In this section, we want to study the dynamics in the NHIM, that is, what are the invariant objects, what is the distance among them in terms of the action I and what are their approximate analytical expressions. This section relies on the proof and the results of Theorem 3.1 in [12], where full details can be found.

We already mentioned in Section 3.1 that the dynamics for the unperturbed Hamiltonian H_0 in (7) (that is, $\varepsilon = 0$) is very simple. Indeed, all the trajectories lie on 2-dimensional invariant tori $I = \text{const}$. The motion on the tori is conjugate to a rigid rotation of frequency vector $(I, 1)$. Notice that the Hamiltonian K is non-degenerate, that is,

$$\frac{\partial^2 K}{\partial I^2} \equiv 1 \neq 0.$$

For $\varepsilon > 0$ small enough, KAM theorem ensures the preservation, with some deformation, of most of the invariant tori present in the unperturbed system. Indeed, those tori having frequencies "sufficiently" non-resonant, which is guaranteed by a Diophantine condition on the frequency vector:

$$|kI - l| \geqslant \frac{\gamma}{|(k,l)|^\tau}, \quad \forall (k,l) \in \mathbb{Z}^2 \setminus \{0\},$$

with $\tau \geqslant 1$ and some $\gamma = \mathcal{O}(\sqrt{\varepsilon}) > 0$. The frequency vectors $(I, 1)$ satisfying this Diophantine condition fill a Cantorian set of measure $(1 - \mathcal{O}(\sqrt{\varepsilon}))\rho$ in any interval of length ρ, called the *non-resonant region*.

Hence, the invariant tori with Diophantine frequencies persist under the perturbation, with some deformation. These KAM tori, which are just a continuation of the ones that existed in the integrable case $\varepsilon = 0$, are commonly known as *primary KAM tori* and are given by the level sets of a function F of the form (see Proposition 3.24 in [12])

$$F(I, \varphi, s) = I + \mathcal{O}(\varepsilon).$$

On the contrary, the invariant tori with resonant frequencies are typically destroyed by the perturbation, creating gaps in the foliation of invariant tori of size up to $\mathcal{O}(\sqrt{\varepsilon})$ centered around resonances (that is, for the values of I such that $kI - l = 0$, for some $(k, l) \in \mathbb{N}^2$ which is the support of the Fourier transform of the perturbation g given in (9)). However, in these resonant regions, other invariant objects are created, such as *secondary KAM tori*, that is, 2-dimensional invariant KAM tori contractible to a periodic orbit, as well as hyperbolic periodic orbits with associated stable and unstable manifolds. To prove the existence of these objects in the *resonant regions* and also to give an approximate expression for them, in [14,12] several steps of averaging were performed before applying the KAM theorem to the Hamiltonian expressed in the averaged variables.

More precisely, given any $(k_0, l_0) \in \mathbb{N}^2$, $k_0 \neq 0$, $\gcd(k_0, l_0) = 1$, for a resonant region centered around a resonance $I = l_0/k_0$, the invariant tori are given by the level sets of a function F, whose dominant term $\bar{F}$ in ε is of the form (see Theorem 3.28 in [12])

$$\bar{F}(I, \widetilde{\theta}) = \frac{(k_0 I - l_0)^2}{2} + \varepsilon k_0^2 U^{k_0, l_0}(\widetilde{\theta}), \tag{47}$$

with $\widetilde{\theta} = k_0 \varphi - l_0 s$. The function U^{k_0, l_0} contains the resonant terms of g with respect to (k_0, l_0), that is,

$$U^{k_0, l_0}(\widetilde{\theta}) = \sum_{t=1}^{M} a_{tk_0, tl_0} \cos(t\widetilde{\theta}), \tag{48}$$

where $M = M(\varepsilon) \geqslant 1$ is an order of truncation of the Fourier series. The lower and upper bounds for the coefficients a_{kl} of g provided by hypothesis (10) ensure that the function (48) reaches a non-degenerate global maximum for any $I = l_0/k_0$ and any $M \geqslant 1$, independently of ε.

Indeed, the function $U^{k_0,l_0}(\widetilde{\theta})$ is analytic and 2π-periodic in $\widetilde{\theta}$. By (10), the function U^{k_0,l_0} in (48) is well approximated by its first order trigonometric polynomial, more precisely,

$$U^{k_0,l_0}(\widetilde{\theta}) = a_{k_0,l_0}\cos(\widetilde{\theta}) + \mathcal{O}_2\big(\rho^{k_0} r^{l_0}\big). \tag{49}$$

As long as ρ, r are small enough, and replacing $\widetilde{\theta}$ by $\widetilde{\theta}+\pi$ if necessary (when $a_{k_0,l_0} < 0$), the function (49) has two non-degenerate critical points corresponding to a global maximum at $\widetilde{\theta} = 0$ and a global minimum at $\widetilde{\theta} = \pi$.

Notice that in the resonant region around $I = l_0/k_0$, the angle variable θ introduced in (38) satisfies $\theta \approx \varphi - (l_0/k_0)s = \widetilde{\theta}/k_0$. Hence, using expressions (47) and (49), the invariant tori in the resonant region are given by the level sets of a function F, whose dominant term F^* in ε can be expressed in the same variables (I,θ) as the scattering map in (41), taking the form

$$F^*(I,\theta) = \frac{(I - \frac{l_0}{k_0})^2}{2} + \varepsilon a_{k_0,l_0}\big(\cos(k_0\theta) - 1\big), \tag{50}$$

which is the Hamiltonian of a pendulum in the variables $(I, \widetilde{\theta} = k_0\theta)$. Notice that a constant term $-\varepsilon a_{k_0,l_0}$ has been added in order that the 0-level set of F^* corresponds to the separatrices of the pendulum.

It is worth noticing that the size in the action I of the region enclosed by the two separatrices of (50), that is, the gap, is given by $\sqrt{\varepsilon|a_{k_0,l_0}|}$. In terms of the variable θ, the function F^* is $2\pi k_0$-periodic and therefore the region enclosed by the separatrices has k_0 components, the "eyes".

We will distinguish two types of resonant regions depending whether the size of the gaps created by the resonances is bigger or smaller than ε.

The resonant region with big gaps is a disconnected set whose connected components are centered around the resonances $I = l_0/k_0$ such that $\sqrt{|a_{k_0,l_0}|} \geqslant \varepsilon^{1/2}$. For these regions we encounter the *large gap problem*. In the regions with big gaps, there are primary and secondary KAM tori, which are given in first order in ε by the level sets of the function (50). The sets where the function (50) takes a positive constant value correspond to primary KAM tori (they are a continuation of the invariant tori existing in the unperturbed case), whereas the sets where the function (47) takes a negative constant value correspond to secondary KAM tori (they did not exist in the unperturbed case).

The resonant regions with small gaps is a disconnected set whose connected components are centered around the resonances $I = l_0/k_0$ such that $\sqrt{|a_{k_0,l_0}|} < \varepsilon^{1/2}$. This case does not present the large gap problem and can be treated analogously as the non-resonant region. Both regions, the small gaps region and the non-resonant region, are called in [12] *the flat tori region* and they contain primary KAM tori given in first order in ε by the level sets of the function

$$F^*(I,\theta) = I, \tag{51}$$

where $\theta = \varphi - Is$.

The result of Theorem 3.1 in [12] provides a sequence of KAM tori $\{\mathcal{T}_k\}_{i=1}^N$, consisting of primary and secondary KAM tori which are $\varepsilon^{1+\eta}$-close spaced, for some $\eta > 0$. Since each invariant torus in this sequence has another invariant torus at a distance smaller than ε, we will see in the next section that it is possible to prove the existence of heteroclinic connections among them using the scattering map (41) (which is ε-close to the identity).

3.4. Part 4. Combination of both dynamics

The geometric mechanism of diffusion close to the NHIM is based on the combination of two types of dynamics, the inner one, provided by Hamiltonian (46) and the outer one, approximately given by the ε time flow of the Hamiltonian (38).

Diffusion inside the 3-dimensional NHIM can only take place between 2-dimensional invariant tori. In order to overcome the obstacles of these invariant KAM tori present in the NHIM, we use the outer dynamics to "jump" from one KAM invariant torus to another one. The 2-dimensional KAM tori in the 3-dimensional NHIM are indeed whiskered tori of Hamiltonian (7), with whiskers inherited from the invariant manifolds of the NHIM. Of course, for this mechanism to be successful, the outer dynamics has to move the whiskered tori, which are invariant under the inner dynamics. More precisely, for any of the KAM invariant tori $\{\mathcal{T}_i\}_{i=1}^N$ given in the previous section, which are $\varepsilon^{1+\eta}$-close spaced for some $\eta > 0$, we want to check that

$$S_\varepsilon(\mathcal{T}_i) \pitchfork \mathcal{T}_{i+1}, \tag{52}$$

where S_ε is the scattering map given in (41). By Lemma 10.4 in [14], condition (52) ensures the existence of a transversal heteroclinic intersection between $\mathcal{T}_i$ and $\mathcal{T}_{i+1}$. In symbols,

$$W^u\mathcal{T}_i \pitchfork W^s\mathcal{T}_{i+1}.$$

Therefore, the sequence $\{\mathcal{T}_i\}_{i=1}^N$ will be a transition chain and from any neighborhood of $\mathcal{T}_1$ and $\mathcal{T}_N$, there exists a trajectory joining them. See Lemma 11.1 in [14].

We have seen that the invariant KAM tori for Hamiltonian (46) are given by the level sets of a function F, having different expressions in the flat tori region and in the big gaps region. Indeed, their dominant term in ε is given by a function F^* that depends only on the variables (I, θ), having expression (50) for the big gaps region and expression (51) for the flat tori region. Moreover, in Eq. (41) we showed that the scattering map S_ε is given in first order in ε by the ε time flow of an integrable Hamiltonian $-\mathcal{L}^*(I, \theta)$ of the form (45).

Considering a whiskered torus of equation inside the NHIM

$$\big\{F(I, \varphi, s) = E\big\},$$

its image under the scattering map is $\{F \circ S_\varepsilon^{-1}(I, \varphi, s) = E\}$, where $F \circ S_\varepsilon^{-1}$ has the following expression:

$$F \circ S_\varepsilon^{-1} = F + \varepsilon\big\{F, \mathcal{L}^*\big\} + \mathcal{O}\big(\varepsilon^2\big). \tag{53}$$

Since the different types of whiskered tori that appear in our problem have different quantitative properties and also different expressions, we consider two different cases to check the transversality condition: the flat tori region and the big gaps region, introduced in Section 3.3.

In the case of flat tori, the dominant term in ε of the function F is given in Eq. (51). Hence, flat tori are given approximately by $I = \text{ctant}$. By expression (53), the image under the scattering map of a flat torus is given in first order in ε by the set of points satisfying

$$I - \varepsilon\frac{\partial \mathcal{L}^*}{\partial \theta}(I, \theta) = \text{ctant}.$$

See Lemma 4.5 in [12] for the technical details.

Because of the "cosine-like" behavior of $\mathcal{L}^*$ described in Proposition 3.9 (see also Remark 3.10), the image of this torus intersects transversally other invariant tori with $I = \text{ctant}$ at a distance smaller than ε. In particular, any other transition torus $\mathcal{T}_{i+1}$ of the sequence, since $\mathcal{T}_{i+1}$ is at a distance $\varepsilon^{1+\eta}$, for some $\eta > 0$.

Notice that depending on the point on the torus that we choose to apply the scattering map, we can "jump" to different transition tori with either a higher or a lower value of the action I. Hence, it is possible to construct several diffusing orbits with increasing or decreasing I.

In the big gaps region the computation is more complex because in this case we have primary and secondary KAM tori. Moreover, the whiskered tori are bent near the separatrix. In a connected component of the big gaps regions, around a resonance $I = l_0/k_0$, invariant KAM tori are given approximately by the implicit equation

$$F^*(I,\theta) = E, \tag{54}$$

for F^* as in (50) and E taking values around 0.

Eq. (54) defines two smooth surfaces given as graphs of the action I over the angle θ defined in a certain range,

$$I = f^*_{\pm}(\theta,\varepsilon) = \frac{l_0}{k_0} \pm \sqrt{2\big(E - \varepsilon a_{k_0,l_0}\big(\cos(k_0\theta) - 1\big)\big)}. \tag{55}$$

When $E > 0$ these smooth surfaces correspond to two primary KAM tori $\mathcal{T}_E^{\pm}$ and the graph (55) is defined in the whole domain $[0, 2\pi)$. For $E < 0$, they correspond to the two components of one secondary KAM torus $\mathcal{T}_E$ and the graph (55) is defined in a domain strictly contained in $(0, 2\pi)$.

By expression (53), the image under the scattering map of a torus in the bigs gaps region is given in first order in ε by the set of points (I,θ) satisfying

$$F^*(I,\theta) - \varepsilon\left(I - \frac{l_0}{k_0}\right)\frac{\partial \mathcal{L}^*}{\partial\theta}(I,\theta) = E. \tag{56}$$

See Lemma 4.7 in [12] for the technical details. Using (55), expression (56) can be written as

$$F^*(I,\theta) \mp \varepsilon\sqrt{2\big(E - \varepsilon a_{k_0,l_0}\big(\cos(k_0\theta) - 1\big)\big)}\frac{\partial \mathcal{L}^*}{\partial\theta}(I,\theta) = E. \tag{57}$$

From expression (57), it is clear that if the second term on the left-hand side, namely

$$\varepsilon\mathcal{M}(\theta,\varepsilon) := \varepsilon\sqrt{2\big(E - \varepsilon a_{k_0,l_0}\big(\cos(k_0\theta) - 1\big)\big)}\frac{\partial \mathcal{L}^*}{\partial\theta}(I,\theta), \tag{58}$$

where $I = -l_0/k_0$, is non-constant, the image of the invariant torus intersects transversally other invariant tori at a distance smaller than ε.

In the case of primary KAM tori (when they are defined as a graph of I over θ in the whole domain $[0, 2\pi)$), there is an easy way to check condition (58). Recall first that, by Proposition 3.9, the function $\theta \mapsto \mathcal{L}^*(I,\theta)$ is "cosine-like" and its dominant term possesses two non-degenerate critical points at $\theta = 0, \pi$. Therefore, one can see that the points on the torus corresponding to $\theta = 0, \pi$ remain invariant for the scattering map, so they are not good for diffusion. However, all the other points are moved by the scattering map. Indeed, for $\theta \in (0, \pi)$, the scattering map decreases the value of the action I, whereas for $\theta \in (\pi, 2\pi)$ the scattering map increases it. See Fig. 6. Again, as in the case of the flat tori region, depending on the point on the torus that the scattering map is applied one can diffuse either increasing or decreasing the value of the action I. In this paper we are concerned with diffusion with increasing I.

Thus, since

$$\frac{\partial^2 \mathcal{L}^*}{\partial\theta^2} \neq 0$$

in $\theta = 0, \pi$, because these points correspond to non-degenerate extrema of $\theta \mapsto \mathcal{L}^*(I,\theta)$, it is immediate that

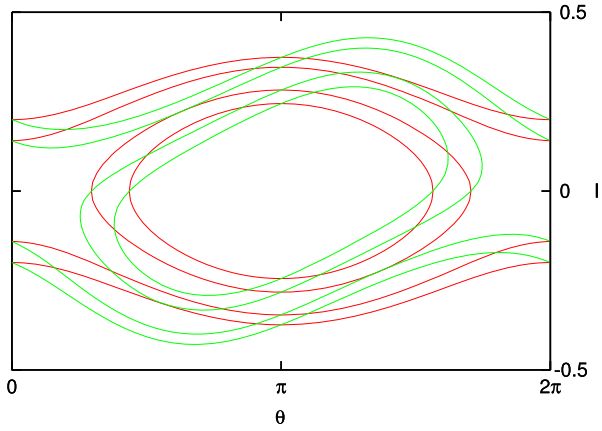

Fig. 6. Primary and secondary KAM tori in the resonant region around $I = 0$ (red curves) given implicitly by the level sets of the function $F^*(I,\theta)$ defined in (50) with $k_0 = 1$, $l_0 = 0$ and $a_{1,0} = 1/2$. Images of these invariant tori (green curves) under the scattering map (41) generated by the reduced Poincaré function $\mathcal{L}^*(I,\theta)$ given in (45). (For interpretation of the references to color in this figure legend, the reader is referred to the web version of this article.)

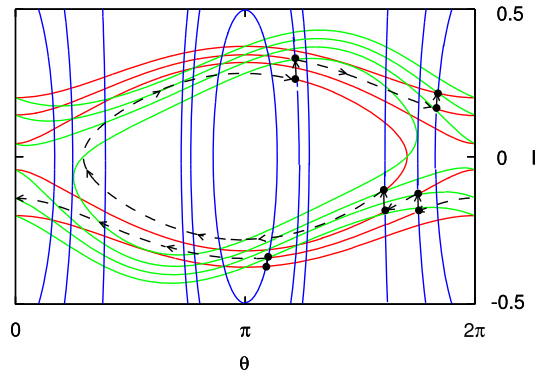

Fig. 7. Illustration of how to combine the two dynamics to cross the big gaps region. Invariant tori for the inner dynamics (red curves) and invariant sets for the outer dynamics (blue curves). Inner dynamics is represented by dashed lines whereas outer dynamics is represented by solid lines. (For interpretation of the references to color in this figure legend, the reader is referred to the web version of this article.)

$$\frac{\partial}{\partial\theta}\mathcal{M}(\theta,\varepsilon) \neq 0,$$

in $\theta = 0, \pi$. Therefore, there exists an open neighborhood around these points where the intersection of the invariant tori with its image under the scattering map is transversal. This is also true for secondary KAM tori in $\theta = \pi$ when k_0 is odd. In the other cases and also in general, it is easy to see in an analogous way that the intersections are transversal because the "cosine-like" behavior of the function $\theta \mapsto \mathcal{L}^*(I,\theta)$ described in Proposition 3.9 guarantees that

$$\frac{\partial}{\partial\theta}\mathcal{M}(\theta,\varepsilon) \not\equiv 0. \tag{59}$$

By means of the combination of two dynamics, we have constructed a sequence of invariant tori in the inner dynamics having transverse heteroclinic connections among them. See Fig. 7 for an illustration of the combination of the two dynamics. Thus, we have constructed a transition chain.

Finally, a standard obstruction property (see [14,18]) shows that there exists an orbit that shadows this transition chain, and Theorem 2.1 follows.

Acknowledgments

We are very grateful to R. de la Llave for the careful reading of the manuscript and valuable advice. We are also thankful to A. Luque, P. Roldán and T.M. Seara for comments and suggestions.

G.H. has also been supported by the i-Math fellowship "Contratos Flechados i-Math", while the final version of this manuscript was written.

References

[1] V.I. Arnold, Instability of dynamical systems with several degrees of freedom, Sov. Math. Dokl. 5 (1964) 581–585.
[2] M. Berti, P. Bolle, A functional analysis approach to Arnold diffusion, Ann. Inst. H. Poincaré Anal. Non Linéaire 19 (4) (2002) 395–450.
[3] M. Berti, L. Biasco, P. Bolle, Drift in phase space: a new variational mechanism with optimal diffusion time, J. Math. Pures Appl. (9) 82 (6) (2003) 613–664.
[4] U. Bessi, L. Chierchia, E. Valdinoci, Upper bounds on Arnold diffusion times via Mather theory, J. Math. Pures Appl. (9) 80 (1) (2001) 105–129.
[5] Sergey Bolotin, Amadeu Delshams, Rafael Ramírez-Ros, Persistence of homoclinic orbits for billiards and twist maps, Nonlinearity 17 (4) (2004) 1153–1177.
[6] L. Chierchia, G. Gallavotti, Drift and diffusion in phase space, Ann. Inst. H. Poincaré Phys. Théor. 60 (1) (1994) 144.
[7] B.V. Chirikov, A universal instability of many-dimensional oscillator systems, Phys. Rep. 52 (5) (1979) 264–379.
[8] C.-Q. Cheng, J. Yan, Existence of diffusion orbits in a priori unstable Hamiltonian systems, J. Differential Geom. 67 (3) (2004) 457–517.
[9] C.-Q. Cheng, J. Yan, Arnold diffusion in Hamiltonian systems: a priori unstable case, J. Differential Geom. 82 (2) (2009) 229–277.
[10] A. Delshams, P. Gutiérrez, Homoclinic orbits to invariant tori in Hamiltonian systems, in: Christopher K.R.T. Jones, Alexander I. Khibnik (Eds.), Multiple-Time-Scale Dynamical Systems, Minneapolis, MN, 1997, Springer, New York, 2001, pp. 1–27.
[11] A. Delshams, M. Gidea, R. de la Llave, T.M. Seara, Geometric approaches to the problem of instability in Hamiltonian systems: an informal presentation, in: W. Craig (Ed.), Hamiltonian Dynamical Systems and Applications, in: NATO Sci. Peace Secur. Ser. B Phys. Biophys., Springer, Berlin, 2008, pp. 285–336.
[12] A. Delshams, G. Huguet, Geography of resonances and Arnold diffusion in a priori unstable Hamiltonian systems, Nonlinearity 22 (8) (2009) 1997–2077.
[13] A. Delshams, R. de la Llave, T.M. Seara, A geometric approach to the existence of orbits with unbounded energy in generic periodic perturbations by a potential of generic geodesic flows of T^2, Comm. Math. Phys. 209 (2) (2000) 353–392.
[14] A. Delshams, R. de la Llave, T.M. Seara, A geometric mechanism for diffusion in Hamiltonian systems overcoming the large gap problem: heuristics and rigorous verification on a model, Mem. Amer. Math. Soc. 179 (844) (2006), viii + 141 pp.
[15] A. Delshams, R. de la Llave, T.M. Seara, Geometric properties of the scattering map of a normally hyperbolic invariant manifold, Adv. Math. 217 (3) (2008) 1096–1153.
[16] A. Delshams, J. Masdemont, P. Roldán, Computing the scattering map in the spatial Hill's problem, Discrete Contin. Dyn. Syst. Ser. B 10 (2–3) (2008) 455–483.
[17] N. Fenichel, Geometric singular perturbation theory for ordinary differential equations, J. Differential Equations 31 (1) (1979) 53–98.
[18] E. Fontich, P. Martín, Arnold diffusion in perturbations of analytic integrable Hamiltonian systems, Discrete Contin. Dyn. Syst. 7 (1) (2001) 61–84.
[19] M. Gidea, R. de la Llave, Arnold diffusion with optimal time in the large gap problem, preprint, 2006.
[20] M. Gidea, R. de la Llave, Topological methods in the instability problem of Hamiltonian systems, Discrete Contin. Dyn. Syst. 14 (2) (2006) 295–328.
[21] M.W. Hirsch, C.C. Pugh, M. Shub, Invariant Manifolds, Lecture Notes in Math., vol. 583, Springer-Verlag, Berlin, 1977.
[22] V. Kaloshin, M. Levi, An example of Arnold diffusion for near-integrable Hamiltonians, Bull. Amer. Math. Soc. (N.S.) 45 (3) (2008) 409–427.
[23] R. de la Llave, A tutorial on KAM theory, in: Smooth Ergodic Theory and Its Applications, Seattle, WA, 1999, Amer. Math. Soc., Providence, RI, 2001, pp. 175–292.
[24] G.N. Piftankin, D.V. Treschev, Separatrix maps in Hamiltonian systems, Russian Math. Surveys 62 (2) (2007) 219–322.
[25] Vered Rom-Kedar, Frequency spanning homoclinic families, Commun. Nonlinear Sci. Numer. Simul. 8 (3–4) (2003) 149–169, Chaotic transport and complexity in classical and quantum dynamics.
[26] D.V. Treschev, Evolution of slow variables in a priori unstable Hamiltonian systems, Nonlinearity 17 (5) (2004) 1803–1841.